Data Analysis for CHAWS Modeling

M. Martinez-Sanchez

Massachusetts Institute of Technology
Department of Aeronautics/Astronautics
Bldg 37-341, 77 Massachusetts Avenue
Cambridge, MA 02139-4307

24 March 2000

Final Report

30 Sep 1993-31 Mar 2000

20030508 075

This technical report has been reviewed and is approved for publication.

DAVID L. COOKE
Contract Manager
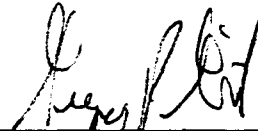
GREGORY P. GINET, Chief
Space Weather Center of Excellence

REPORT DOCUMENTATION PAGE

1. REPORT DATE *(DD-MM-YYYY)*

2. REPORT TYPE

3. DATES COVERED *(From - To)*

4. TITLE AND SUBTITLE
Data Analysis for CHAWS Modeling

5a. CONTRACT NUMBER
F19628-93-K-0029

5b. GRANT NUMBER

5c. PROGRAM ELEMENT NUMBER
63410F

6. AUTHOR(S)
Manuel Martinez-Sanchez

5d. PROJECT NUMBER
2822

5e. TASK NUMBER
02

5f. WORK UNIT NUMBER
03

7. PERFORMING ORGANIZATION NAME(S) AND ADDRESS(ES)
Department of Aeronautics/Astronautics
Massachusetts Institute of Technology
77 Massachusetts Avenue
Cambridge, MA 02139-4307

8. PERFORMING ORGANIZATION REPORT NUMBER

9. SPONSORING/MONITORING AGENCY NAME(S) AND ADDRESS(ES)
Air Force Research Laboratory/VSBXS
29 Randolph Road
Hanscom aFB, MA 01731-3010

10. SPONSOR/MONITOR'S ACRONYM(S)

11. SPONSOR/MONITOR'S REPORT NUMBER(S)
AFRL-VS-TR-2002-1616

12. DISTRIBUTION/AVAILABILITY STATEMENT
Approved for public release; distribution unlimited

13. SUPPLEMENTARY NOTES

14. ABSTRACT
We report here on results on two related areas of plasma-structure interaction: the analysis of data on ion collection by a negative probe in the wake of large objects (CHAWS experiment), and the modeling of electron collection by a bare positive tether in a low Earth orbit. In the first area, our analysis contributed to a number of important conclusions, including the identification of a probable density probe miscalibration, quantification of the role of H= ion collection (particularly at low bias), and description of the cylindrical-to-spherical probe sheath transition as bias increases. In the tether modeling ara, we have been able to move beyond the classical analysis of Laframboise for a non-moving, non-magnetized cylindrical probe by including both a meso-thermal plasma flow, and a cross-magnetic field, both representative of orbital conditions. The full Particle-in-Cell codes we developed predict that, in the presence of the cross-flow, current collection exceeds the Orbital Motion Limit by a factor close to 2. Preliminary analysis of these results indicate that the strong plasma fluctuations revealed by the simulation in the frontal (ion stagnation) area are responsible for the current excess.

15. SUBJECT TERMS
Plasma sheaths
Langmuir probe
Mathematical modeling

16. SECURITY CLASSIFICATION OF:

a. REPORT	b. ABSTRACT	c. THIS PAGE
UNCL	UNCL	UNCL

17. LIMITATION OF ABSTRACT
UNL

18. NUMBER OF PAGES

19a. NAME OF RESPONSIBLE PERSON
David Cooke

19b. TELEPHONE NUMBER *(Include area code)*
(781) 377-2931

CONTENTS

ILLUSTRATIONS

Final Technical Report on Contract no. F19628-93-K-0029
DATA ANALYSIS FOR CHAWS MODELING
by Manuel Martinez-Sanchez, MIT, Aero/Astro
March 24, 2000

Abstract

We report here results on two related areas of plasma-structure interaction: the analysis of data on ion collection by a negative probe in the wake of large objects (CHAWS experiment), and the modeling of electron collection by a bare positive tether in a low Earth orbit. In the first area, our analysis contributed to a number of important conclusions, including the identification of a probable density probe miscalibration, quantification of role of H^+ ion collection (particularly at low bias), and description of the cylindrical-to-spherical probe sheath transition as bias increases. In the tether modeling area, we have been able to move beyond the classical analysis of Laframboise for a non-moving, non-magnetized cylindrical probe by including both a meso-thermal plasma flow, and a cross-magnetic field, both representative of orbital conditions. The full Particle-in-Cell codes we developed predict that, in the presence of the cross-flow, current collection exceeds the Orbital Motion Limit by a factor close to 2. Preliminary analysis of these results indicate that the strong plasma fluctuations revealed by the simulation in the frontal (ion stagnation) area are responsible for the current excess.

1 Introduction

The subject matter of this Contract comprises two different, but interrelated topics: (a) Analysis of the data on wake-side ion currents during the two CHAWS flight experiments, and (b) Development of a computational method for calculating the electron current collection by a positively biased bare orbiting tether. Topic (a) was supervised by Prof. Daniel E. Hastings, and primarily executed by his Graduate Research Assistants Graeme Shaw and Gregory B. Giffin, plus Post Doctoral Associate Dr. Gabriel Font. When Prof. Hastings took a leave of absence from MIT in order to serve as Air Force Chief Scientist (Sep. 1997-Sep. 1999), supervision of this contract and its extensions passed to Prof. Manuel Martinez-Sanchez, who, with his Graduate Research Assistant Tatsuo Onishi, pursued mainly topic (b) above.

In this Report we summarize the results of these efforts and make reference to the publications and Theses where more detailed accounts can be found. Section 2 covers the CHAWS analysis, and Section 3 refers to the tether code development.

2. Data Analysis For The Plasma Wake Ion Currents During The Chaws (Changing Hazards And Wake Studies) Experiments

2.1 Background

The Wake Shield Facility (WSF) free-flyer was released from the Space Shuttle during two separate flights (STS-60 and STS-69). It consisted of a 3.6 m. diameter disk flying in a head-on configuration in order to create a high vacuum wake in which several experiments could be conducted. One of these was CHAWS, which consisted of a cylindrical Langmuir probe (0.45m long, 0.10m diameter) inside the wake, plus a ram-

side sensor used to characterize the plasma environment. The overall configuration is shown in Figure 1. The purpose of the
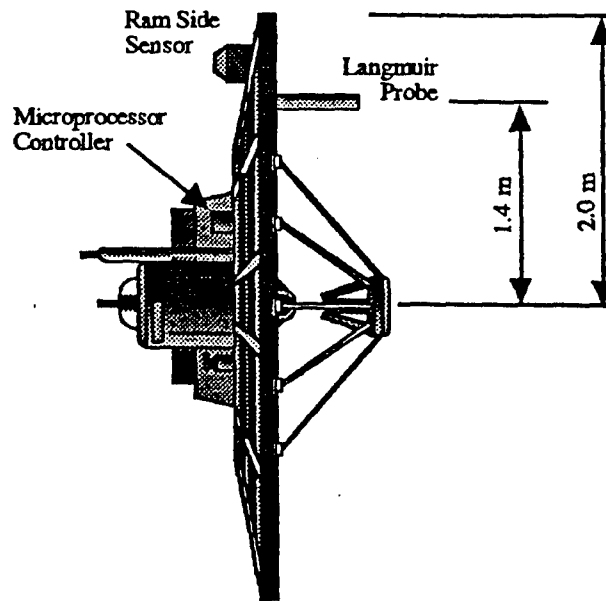
Figure 1: CHAWS components mounted on the WSF.

experiment was to characterize the rarefied plasma behind the plate, particularly regarding ions that may be attracted to any negatively biased object in that region.

CHAWS I flew in February 1994, and, due to hardware difficulties did not separate from the Shuttle, although it was able to obtain data while the WSF was held aloft by the manipulator arm. In addition, negative probe voltages were limited to no more than –125V by a power supply short. CHAWS II flew successfully in Sep. of 1995 and was able to collect data spanning a large range of voltages, environmental conditions and flight altitudes.

Several analytical and numerical tools were available from previous work to help reduce and analyze the collected data. The Ram-Side Sensor RPA calibration went through a post-flight iteration, which necessitated a re-analysis of the data from CHAWS I (done originally by G.B. Shaw[11]) by G.B. Giffin[2]. The second, and more accurate, calibration was worked out by Dr. D.L. Cooke, and is reported in Appendix A of Giffin's Thesis [2]. Data processing and displaying software (CHAP and CHUNKS) was also available from the Hanscom AF Phillips Laboratory work. In addition, a hybrid PIC Code developed at MIT by Dr. G. Font was also used extensively in the course of this work.

2.2 Results and Analysis

The complete set of experimental results were reported in Refs. 4 and 5. Following re-calibration, as mentioned above, data from CHAWS I and II agreed well for the low-voltage range where they overlapped. A first correction that proved important was the removal of the probe secondary electron current, especially at high bias voltages. This secondary current was estimated on the basis of a limited set of emission coefficient data for the same material that had been obtained elsewhere [6]. After this correction, the current-voltage data trend was linear above some 20 Volt bias, as expected from

2

simulations and from spherical Orbit Motion Limit (OML) theory (as noted below, end effects made the cylindrical probe behave as effectively spherical).

Comparisons to PIC code simulation results [2,3] indicated a current under-prediction by factors of the order of 2 (Figure 2). The code was calibrated against POLAR and yielded identical results for equal inputs. The electron temperature uncertainty was ruled out as a cause of significant error, due to it insensitivity for near OML conditions.

One potential reason for current under-prediction was the omission by the codes of any H^+ contribution (only O^+ was considered). The very light H^+ ions would be expected to turn much more easily towards the negative probe, and could contribute out of proportion to their relative abundance. A series of PIC simulations [2,3] established that H^+ (if present at a 5% level) could indeed be a significant current carrier at low bias voltages below≈100V, (but could not explain the large discrepancies at higher voltages (up to 3000V).
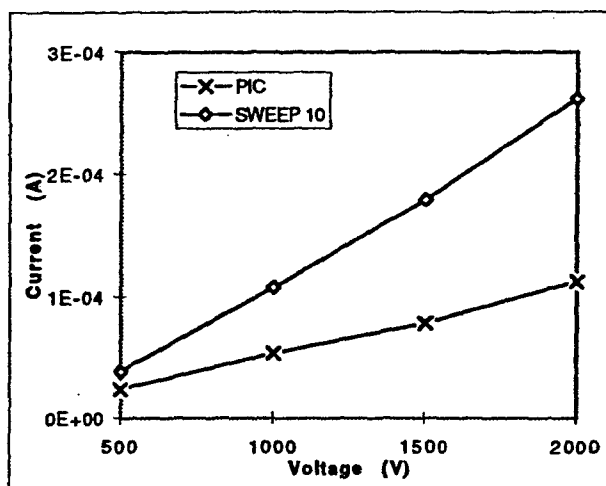
PIC-Data comparison for sweep 10 (CHAWS I).
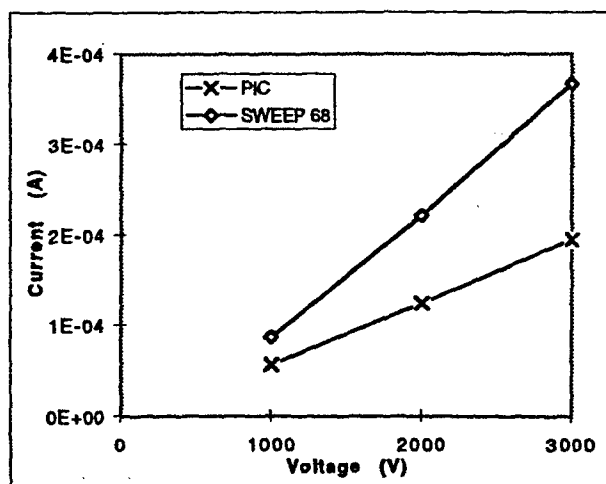
PIC-Data comparison for sweep 68 (CHAWS II).

Figure 2: Comparison between PIC simulations and Data.

It was therefore suspected that the n_∞ data from the Ram-Side Sensor were systematically low. This was reinforced by comparison of the sensor's results of n_∞ to the IRI ionospheric model, which again, showed under-determination by factors of about 2 (Figure 3). A systematic process of n_∞ and T_e adjusting, using the data from the probe when in a ram configuration, yielded estimates for these parameters that were 1.8 to 2 times those of the ram sensor, and also estimates of T_e that were 4-6 times T_i, higher than the expected 1.5 T_i . With these revised parameters, agreement between data and code results was restored throughout the bias range. The actual H^+ concentration is very sketchily known, estimates ranging from 0.1% to 30% (Ref. 3). In view of this, the low-voltage current data, which should be dominated by H^+, were compared to PIC simulations at varying H^+ concentration, and an H^+ concentration estimate was derived from this process (1.3±0.8%).

Confidence in the code and its interpretation was boosted by its successful prediction of the "turn-on" voltage level, namely, that bias for which the probe sheath would begin to protrude into the free-stream (wake configuration). Below this voltage, only H^+ could be collected, with a smaller I(V) slope. An example of this behavior is shown in Figure 4 (from simulations) and in Figure 5 (from data).
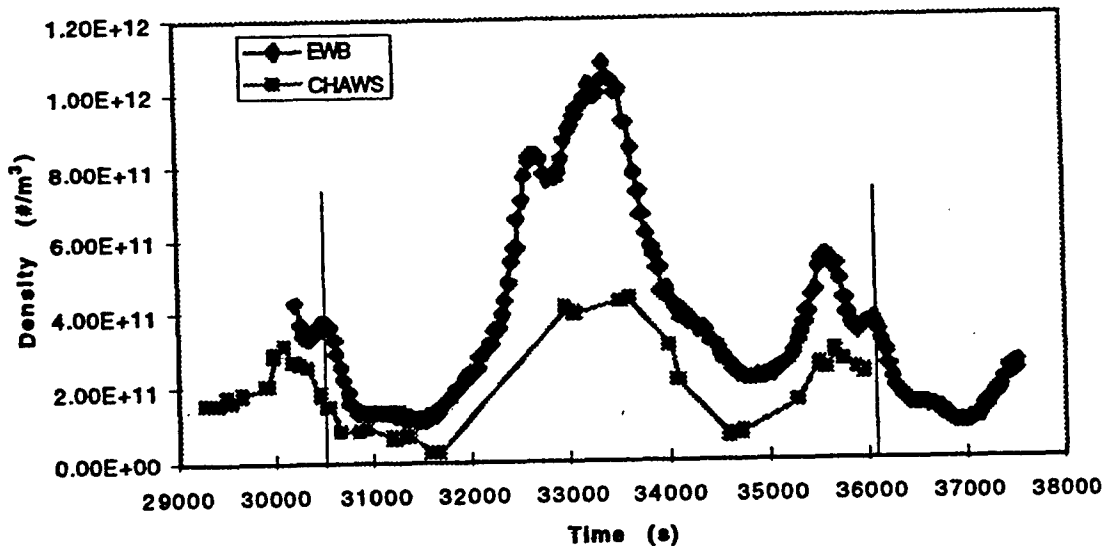

Figure 3: Comparison between CHAWS density values and the IRI model. The two vertical lines enclose one period of the data.
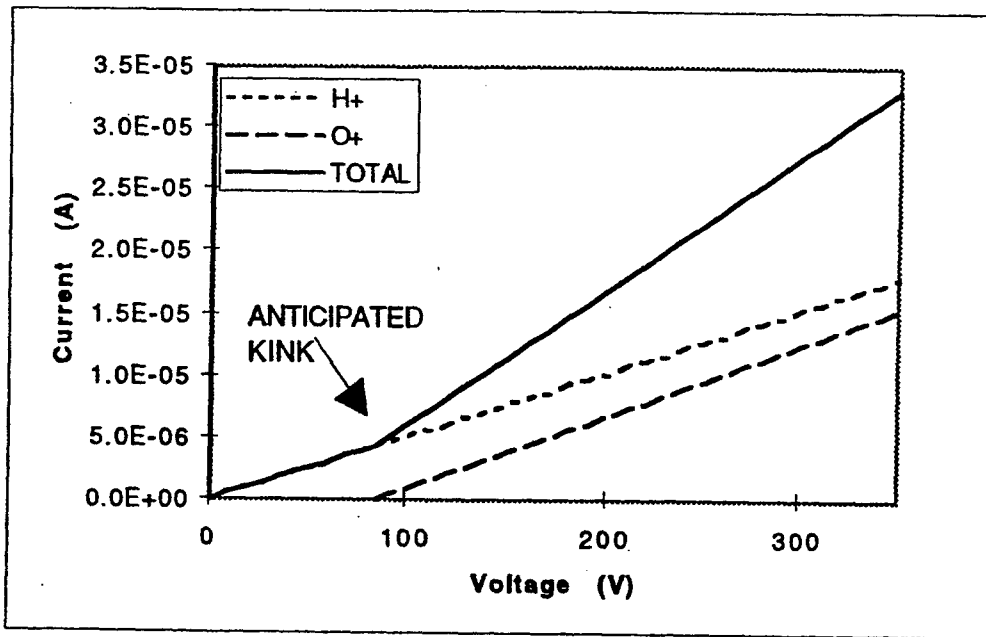
4

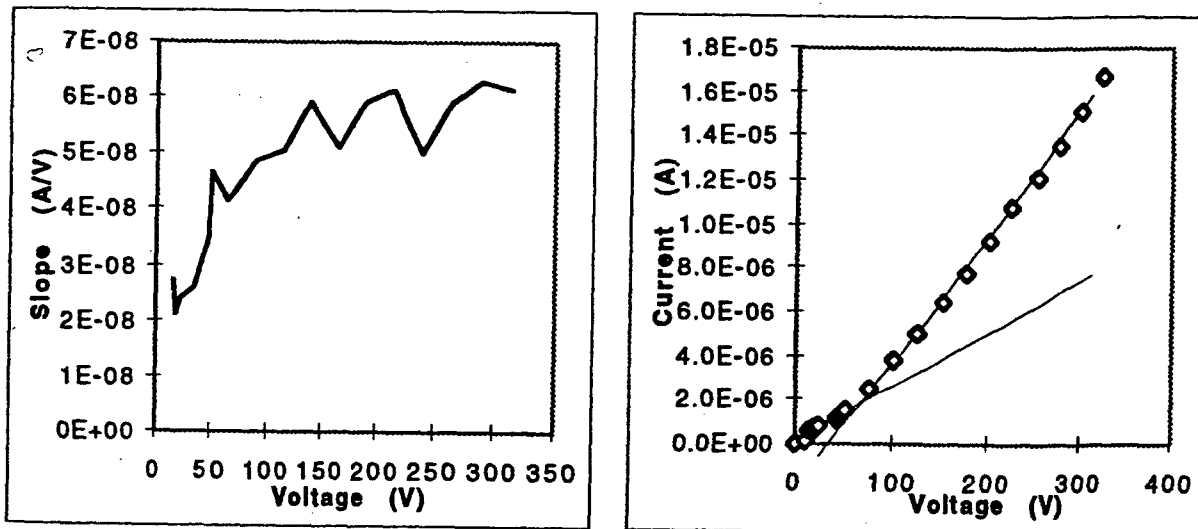**Fig. 4: Superposition of extrapolated O+ and an H+ (figure PIC trials).**

Figure 5: Turn-on location for step 52

In addition to these effects, the PIC simulations provided a wealth of information and insights into the physics of the ion collection in the wake. These include:

-Verification that the probe sheath grows to beyond the shield's rim as the bias increases. The size of the protruding region can then be used for a simple analytical collection model.
-Verification that the region behind this protrusion is drained of ions, and that these ions all focus on nearly the same spot on the back side of the probe.
-Visualization of the growth of the probe sheath from cylindrical at low bias to nearly hemispherical at large bias. As a consequence, Laframboises's cylindrical probe theory substantially underpredicts the current.

Details of these analyses can be found in [2] and [3].

In summary, the work under this Contract has materially contributed to the proper interpretation of the experimental data from CHAWS, and has advanced the level of scientific prediction and engineering understanding of the complex phenomena occurring in the near-body wake region.

3. Development of a Computational Method for Current Collection by a Bare Tether

3.1 Background

The concept of the space tether is now common knowledge within the scientific community and has existed for several decades. The proposed uses for space tethers include ULF antenna[7], orbital momentum transfer, spacecraft power/propulsion, and the more speculative space elevator/skyhook[8,9]. The first part of the proposed research concentrates on the electrodynamic tether. Martinez-Sanchez et al (1987)[10] have categorized the various uses of the electrodynamic tethers, identified the primary competing technology for each use, and performed a first order systems study comparison between each. The results are summarized below in Table 1.

Table 1: Potential Applications of Electrodynamic Tethers
(Martinez-Sanchez et al, 1987)

Application	Competing Technology	How Tether Compares
Orbital inclination, altitude changes, drag compensation	Chemical or electrical rockets	Comparable or better
Emergency power with altitude loss	Batteries, fuel cells	Favorable depending on power conditioning
Power generation with rocket assist	Fuel Cells	≈twice as good
Orbital energy storage for solar arrays	Batteries, regenerative fuel cells	Comparable but some tether dynamics difficulties

This and other similar systems studies in the pre-TSS era were characterized by large uncertainties which prevented definitive statements of tether performance. Chief among these uncertainties were ionospheric circuit impedance, collection characteristics of tether anodes, and other systems issues such as retrieval dynamics and long term thermal control.

Fortunately, aside from the mentioned difficulties, much of the critical tether physics is straightforward. The motion of a long conducting tether through the Earth's magnetic field generates a potential difference across the tether which is given by

$$V_{emf} = \left| \vec{V_o} \times \vec{B} \cdot \vec{l_{th}} \right|$$
(1)

If a current is allowed to flow across this difference, say by providing the tether with plasma contractors, then the tether experiences a Lorentz, or drag, force which opposes its orbital motion and is given by

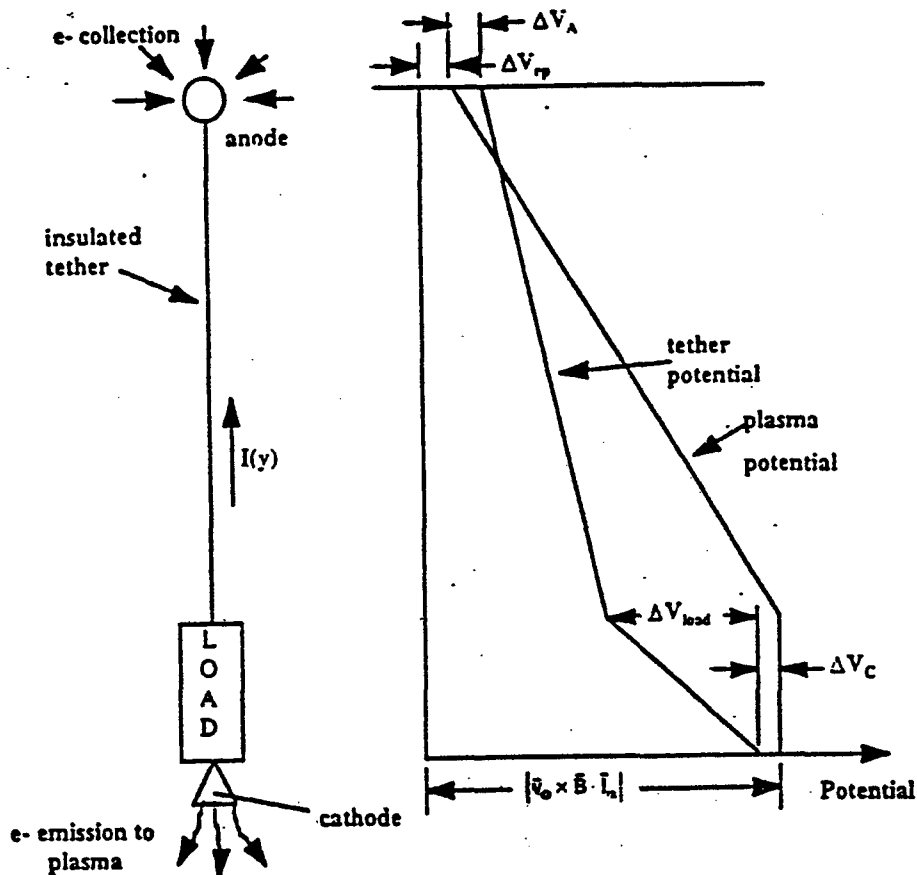$$\vec{D_{th}} = (\vec{l_{th}} \times \vec{B})I$$
(2)

Figure 6: Potential diagram for 'standard' (TSS) tether as a Generator (upwards deployed).

The tether generator equation, accounting for the contactor potential drops (ΔV_A and ΔV_C), the load to be powered, and the ionospheric resistance (ΔV_{RP}), is given by

$$V_{emf} = \Delta V_A + I_{th} + IR_{load} + \Delta V_C + IR_{RP} \qquad (3)$$

Over both the orbital and daily periods there are substantial variations in the geomagnetic field, B, and also in the plasma density, through which the tether system must complete the circuit in order to drive a current. These variations complicate the design and optimization of tethers and must be considered in any meaningful comparison to other power/propulsion alternatives. The physics of a propulsive tether is essentially identical only the tether is deployed downwards and onboard power is applied to overwhelm the induced emf and, by equation (2), add energy to the spacecraft's orbit.

An inherent advantage of tethers over its competitors which is not immediately obvious from the above table is *flexibility*. One tether aboard a spacecraft can act as a battery, a power supply, a thruster, or an augmented fuel cell. The promise demonstrated by the various systems studies, the simplicity of much of the tether physics, and the inherent flexibility offered by an electrodynamic space tether has been sufficient to spur several sub-orbital tether flights and two LEO flights (TSS-1 and TSS-1R).

Recent studies have demonstrated the potential for large savings if an electrodynamic tether is used for drag make-up on the International Space Station[11,12,13], Table 2, from Ref. 12, shows that if the average Space Station drag is 0.7N, the ED tether system saves over 10 years minimum of $10 \times 0.7 \times (24.7-10) = \$103M$ (in comparison to an ion engine system). In comparison to a chemical thruster system, as presently planned for the space station, the savings approach one billion dollars.

Table 2. Reboosting Costs per year (M$/yr/N)

	Propellant	Power	Hardware	Total
Chemical	146.0	-	-	146.0
Ammonia Arcjet	60.2	1.0	2.2	63.4
Xe Hall	30.1	1.4	4.4	35.9
Xe Ion	18.5	1.8	4.4	24.7
ED Tether	1.5	1.3	7.2	10.0

One key feature of the system evaluated in Refs. 11 and 12 is the use of a bare tether for electron collection at the positive end of the tether. This has two types of advantage: (a) Simplicity and mass savings, by eliminating the need for an active gas expulsion system (plasma contactors) or a large solid collector (TSS), and (b) Robustness against large ionospheric plasma density fluctuations. The latter point is well illustrated by Figure 7 (from Ref. 12): one full order of magnitude change in density, as in day-night variations, results in a 10-15% change in tether current, and hence in thrust. This is a result of the self-adjusting nature of the length of tether which is positive with respect to ambient: at

8

low plasma densities, this part of the tether expands, and the extra collecting length nearly compensates for the reduced collection per unit length.
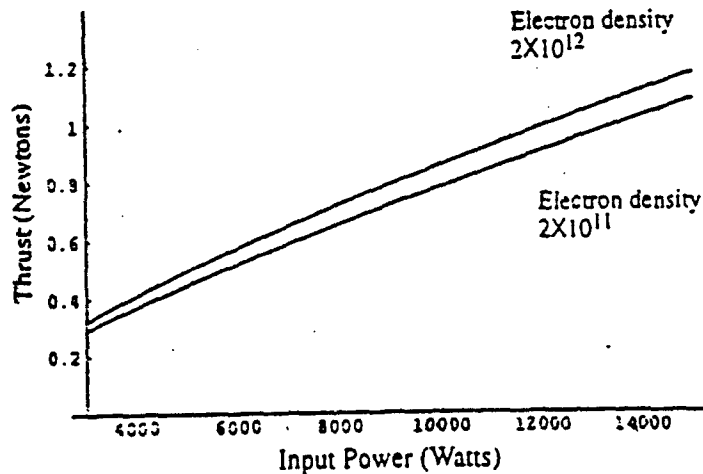

Fig. 7: Variation of thrust.

Predictions such as those embodied in Fig. 7 are based on existing theories of electron collection by probes. These theories are largely limited to spheres, cylinders or planar surfaces in contact with collisionless, Maxwellian plasmas at rest. Prominent among them is the work of Laframboise[14]. More specifically, preliminary design work being carried out for a bare tether demonstration mission by NASA (Marshall S.F.C.)[15] is based on a particularly simple limiting form of this classical theory, the so-called Orbital Motion Limit. This is the case of an un-shielded charge collector, in which the collection rate for a given object is only limited by the fact that attracted particles will miss the object if their angular momentum is excessive for a given energy. Approximate arguments were advanced in the original bare tether literature[16] to justify the use of OML expressions for tether design, and these arguments have more recently [17,18] been sharpened and extended to non-circular geometries. However, classical theory and its extensions cannot readily deal with the full set of conditions encountered by an orbiting tether, such as plasma cross-flow, magnetization, arbitrary geometries, and possible instabilities.

3.2 The Tether Anode Problem

As noted, sections of a bare tether with a positive potential bias will act as electron collectors (anodes). In this section we will review the physics of this collection and the modeling idealizations which can be used for its analysis. We will proceed from the simplest useful abstraction and sequentially introduce the various complications.

(3.2a) Plasma at rest, no magnetic field. OML conditions

As we mentioned in Section 1, the OML limit applies when shielding can be ignored. This implies (Size) << (Debye length), but more detailed analysis[17] shows that it holds up to where the two quantities are comparable. This regime, if it applies, is simplest to analyze, because the current collection formulae can be shown[19] to be *universal*, i.e., the same current is collected per unit probe area by any 2-D probe as long

9

as it operates in the OML regime. For the practical case where the probe bias Vp is much more than the electron temperature kT_e/e, the current per unit length is simply

$$\frac{dI}{dy} = \frac{P}{\pi} en_e \sqrt{\frac{2eV_p}{m_e}} \quad \text{(OML, any 2-D shape)} \qquad (4)$$

where (P) is the perimeter of the 2-D probe. Aside from this simplicity, the interest of the OML regime resides in the fact that it gives an upper bound to the possible collection rate, because any shielding will necessarily reduce collection by "hiding" the probe from a segment of the electron population.

(3.2b) Plasma at rest, no magnetic field. Partial shielding

As the probe size (cross-section) increases, or as the plasma density increases for a given size, some outlying portions of the plasma that would in principle contribute electrons to the attracting probe become electrostatically shielded away from it by the charge redistribution it induces. The current then drops below the OML limit (Eq. (4)). On the opposite limit, the presence of the probe is only felt within a very thin sheath, and simplicity is recovered in the form of the locally-flat probe expression.

$$\frac{dI}{dy} = Pen_e \sqrt{\frac{kT_e}{2\pi m_e}} \quad (\lambda d << R, \text{ any shape}) \qquad (5)$$

which is smaller than the OML current by $\sqrt{\dfrac{4}{\pi} \dfrac{kT_e}{eV_p}} << 1$

The analysis for intermediate conditions is only feasible for circular cylinders[14], and even then it requires iteration between electron trajectory integrals and solutions of Poisson's equation.

(3.2c) Flowing plasma, no magnetic field

In orbit, the plasma speed relative to a tether is on the order of 7.6 km/s. Since $T_e \sim T_i \sim 0.1eV$ the thermal velocities of electrons and ions (O+) are, respectively, 210 Km/s and 1.2 Km/s. Thus, the plasma motion would by itself introduce only a very small perturbation on the electron collection, were it not for the strong electrostatic coupling of the electrons to the ions, which are themselves hypersonically streaming past the tether. Because of this streaming, an ion-depleted wake forms behind the obstacle, and this wake must acquire a potential of the order of a few times $(-kT_e/e)$, sufficiently negative to keep electrons out as well. Conversely, the ion inertia will induce some sheath thinning on the front side of the probe.

10

The symmetry being broken, the problem is now fully 2-D, and no analytical solution is possible. One could expect some reduction of the electron current, because few electrons will penetrate to the cylinder's rear side; on the other hand, a higher ion energy tends to extend the OML range in the non-flowing case[16], and some reflection of this effect may also tend to increase electron collection when the ion energy is directed. Resolution of this dilemma must rely on numerical solutions, such as those proposed below.

(3.2d) Flowing, magnetized plasma

Order-of-magnitude analyses in Ref. 17 indicate that magnetic effects should remain small provided the electron thermal gyroradius, ℓ_e, is greater than both the cylinder's radius and the Debye length. These conditions are satisfied in the ionosphere (ℓ_e~25 mm, λ_D~7 mm, tether radius~1 mm). On the other hand, it is difficult to estimate the effects to be expected from the extended "wings" that will propagate some of the probe's positive potential along the intercepted magnetic lines. This effect results from the preferential draining of electrons along the B field direction, leaving behind some excess positive charge.

The dynamics of these wings is quite complex, and no satisfactory theory for them exists at this time. In the case of a spherical anode, Laframboise[20] has argued that the intercepted magnetic stream tubes are half-depleted of electrons for some substantial length. These depleted regions rise to fairly large potentials, and then scatter ions to maintain quasi-neutrality. A region of higher (~30%) plasma density results in front of the magnetic wing, which substantially modifies the current collected by the probe, yielding factors of 2-3 above the classical Parker-Murphy[22] estimate.

In a related study, also addressed to the spherical case, Cooke and Katz[21] introduce the idea of a "heated presheath", whose higher thermal current would lead to 3-4 times higher current than Parker-Murphy for TSS-1R conditions. The energy for this presheath heating ultimately derives from the ions' ram kinetic energy. Since pre-sheath electrons are nearly trapped in the electrostatic potential hump in front of the probe (of the order of $\phi \approx m_i v_i^2 / 2e \approx 5$ *volts* their energy can be thermalized to $T_e \sim \frac{2}{5} e\phi / k \sim 2eV$ which is of the order required to explain the current enhancement.

Arguments similar to those of Refs. 20 and 21 are more difficult to construct for a 2-D geometry, such as a tether. An extended electron-depleted wing would in this case resemble a "wall" or slab of a thickness defined by the radius of the tether's sheath, and ions cannot scatter around its high potential, as in the spherical case. In fact, the effect of a high-potential slab would in this case be to slow the ions down as they traverse it, further *increasing* the excess positive charge. Either some other mechanism must aid in the formation of a moderate-potential pre-sheath (perhaps the creation of localized tether-aligned plasma currents), or unsteadiness may be inevitable. In either case, detailed numerical simulation offers the only reasonable hope of clarification.

3.3 Numerical Methods

3.3.1 PIC vs. Boltzmann methods

Of the many numerical techniques available for plasma modeling (Ref. 23), the Particle-in-Cell (PIC) method[24] is the most widely used when collisionality is negligible. Ions and electrons are lumped into macro-ions and macro-electrons with their physical charge/mass ratio, but with a mass chosen such as to have a reasonable number (~20 or 30) per numerical grid cell at all times. Potentials and field components are computed at grid nodes. In each computational cycle, these fields are interpolated to the current positions of each charged macro-particle, and the charges' velocities and positions are accordingly advanced using an appropriately short time-step. Following this, the charges are back-interpolated to the grid nodes, and one or a few iterations performed on the Poisson equation to update the fields. The procedure is repeated, typically for thousands to tens of thousands of cycles.

The grid used for PIC computations is most often rectangular, which facilitates interpolations. The grid spacing must resolve the local Debye length, after which the number of macro-particles is chosen, as noted, to yield good statistics. The time step must be shorter than the flight time through one grid cell, and must also resolve plasma-frequency oscillations.

One significant simplification that occurs in the symmetric case (no flow, no magnetic field), and when $eV_p/kT_e \gg 1$ is that, regardless of the mass ratio m_e/m_i, the ion population accurately follows Boltzmann's relation.

$$n_i = n_\infty e^{\frac{e\phi}{kT_i}} \tag{6}$$

This relation is mass independent. The implication is that correct steady state results will be obtained even if m_i/m_e is greatly different from its physical value of 29,600. Our no-flow results were obtained with $m_i/m_e = 1$, and verification runs at different m_i/m_e values confirmed the invariance. Using either Eq. (6) or moving ions with $m_i/m_e = 1$ greatly reduces the computational burden; with the correct m_i/m_e, ions move very little in one electron passage-time, and many such passage-times need to be spanned to ensure a proper ion distribution.

With a non-zero ion velocity far from the probe, Eq. (6) is not valid, because $\frac{1}{2}m_i\left|\vec{v_i} - \vec{v_{i\infty}}\right|^2 + e\phi$ is not a constant of the motion, and hence a translating Maxwellian does not satisfy Vlasov's equation. Because of this, the real $\frac{m_i}{m_e}$ value must be used, which has the effect of significantly slowing down the computation since ions move very little in one electron passage time.

Some consideration has been given to alternative computational methods, particularly those which directly solve the Vlasov-Poisson set of partial differential

equations in phase space. In these methods, there is no need to store the positions and velocities of each of the 20,000-200,000 macroparticles used in PIC. On the other hand, each velocity component must be either discretized into a velocity-space grid (at each spatial node), or else the distribution in each velocity component must be represented by a sufficient number of basis functions, usually Hermite functions[27], whose coefficients become the velocity variables. For our problem, assuming only two velocity components need to be tracked, and that, following Ref. 27, 64 base functions per component are sufficient, this represents 4096 variables per spatial grid point, per time step. A typical grid, from Ref. 26, contains about 3000 nodes, for a total of roughly 12 million variables per time step. For comparison, the PIC simulations of Ref. 26 used typically 200,000 macroparticles, whose two position and two velocity components were recorded at each time step. Including the field variables, this amounts to fewer that 1 million variables. It appears therefore that Vlasov methods are more memory-intensive than PIC methods, although a more careful comparison *at equal accuracy* might reduce or erase their difference. Perhaps more significant as a deterrent is the much greater formulation effort required for Vlasov methods, where a variety of spectral coefficients must be pre-calculated for each basis function selection, and, as Ref. 27 discusses, judgment must be used in selecting basis sets which are appropriate to each problem: for example, Hermite functions may be appropriate for electrons, but not for the streaming ions in our problem. For these reasons, we have baselined PIC as the methodology of choice, the decision to be revised only if what appear to be insurmountable numerical issues, mainly related to precision, were to arise.

3.3.2 PIC Solutions with no flow or magnetic field.

In our initial numerical work on the bare tether problem [25,26], we adapted the PIC model to the cylindrical geometry of a region surrounding the cross-section of a tether, and performed extensive verification computations for the simple case of a circular cross-section and no cross-flow or magnetic field. The cases studied straddle the OML limit, ranging from $R/\lambda_d = 0.2$ to $R/\lambda_d = 5$. The assumed probe potential was $eV_p/kT_e = 25$, the highest reported in the solutions of Ref. 14, which were used for verification.

In the absence of ion flow, a neutral pre-sheath must form in order to accelerate electrons to their ambipolar speed of sound at the edge of the high-voltage sheath. The radius of this presheath is in general larger than that of the computational domain, which means that the potential and the field are non-zero at this latter radius, and must be specified carefully to avoid biasing the resulting current. Our method consisted of explicitly imposing quasi-neutrality at the computational boundary[26], which is always outside of the sheath edge. The ion density is related to potential through a simple Boltzmann factor, the density of incoming electrons can be computed analytically as a function of potential, and that of outgoing electrons is taken from the numerical flux and mean velocity at the previous time step. Equating the ion density to the sum of the two electron densities yields the proper edge potential at each time.

Figure 8 shows an example of the calculated potential distribution for $R/2d = 1$. Figure 9 compares the numerical results to those of Laframboise[14] for a range of R/d_D values. The OML limit is approached for $R/d_D < 1$. Our results follow the theoretical

trend well, although there is a consistent under-calculation of current of about 10%, due probably to distortions introduced by the non-rectangular grid[26].
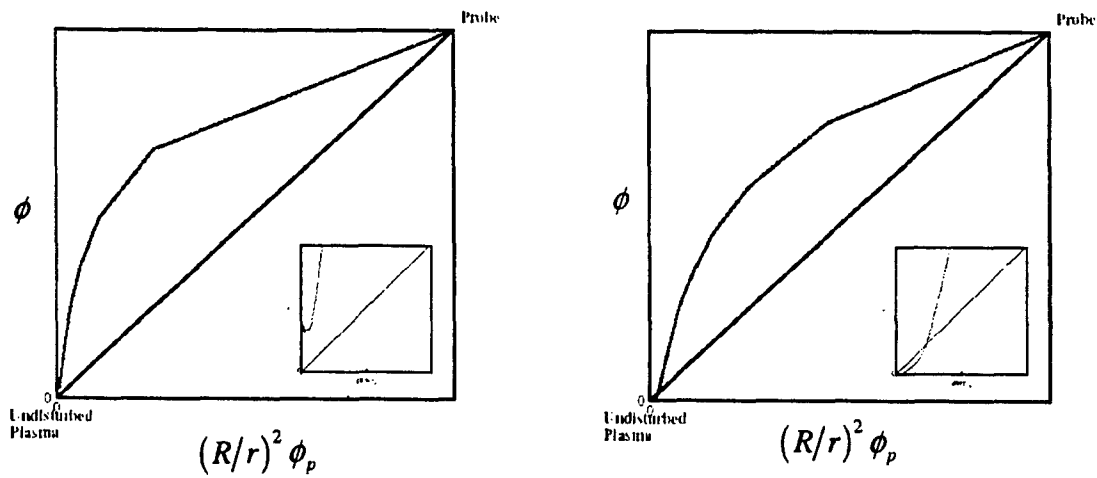
(a) Very small probe radius ($\frac{r_p}{d_D} = 0.5$) : well in the OML regime

(b) Small probe radius ($\frac{r_p}{d_D} = 1$) : in the OML regime
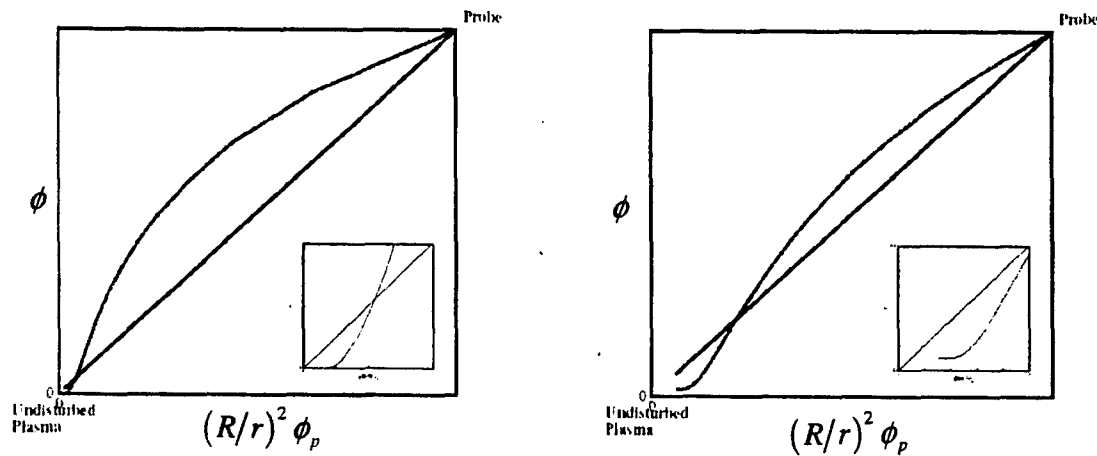
(c) Medium probe radius ($\frac{r_p}{d_D} = 2$) : near the OML regime

(d) Large probe radius ($\frac{r_p}{d_D} = 5$) : out of the OML regime

Figure 8: Calculated potentials distributions for various values of R/d, plotted versus $(R/r)^2$, as suggested in Ref. 17. The inset figures are close ups of the lower left portion of the plots, the undisturbed plasma.
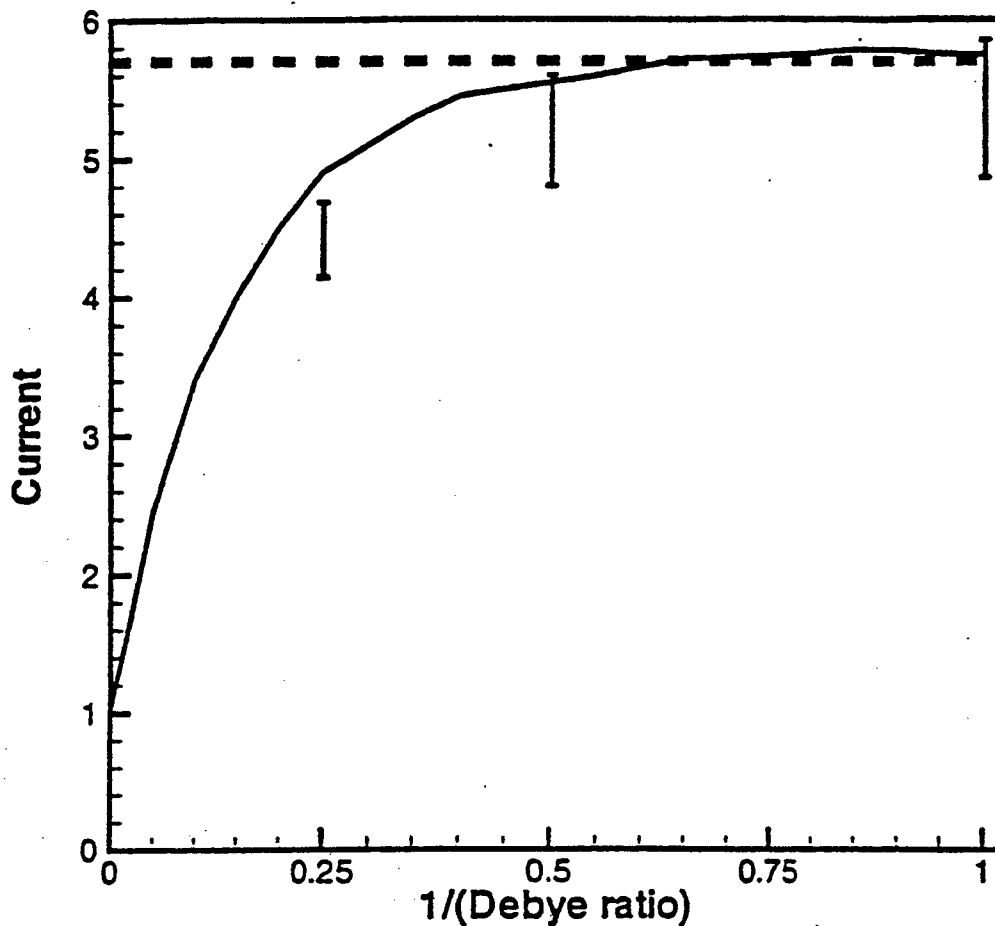
14

Figure 9: Current collection vs $1/\xi_p = d_D/R$. OML current (dashed), the exact value (solid) and computed value (error bars).

3.3.3 PIC Solutions with flow and magnetic field

Our more recent work[28] has concentrated on the more numerically demanding cases when the symmetry is broken by a high-speed plasma cross-flow, as in the real orbiting-tether situation, as well as by the presence of a $\vec{B}$ field strong enough to magnetize the electrons. Not only is the symmetry lost, but, the real m_i/m_e showed a greatly enlarged frontal portion of the tether sheath, since ions are deflected at a lower potential. With the current m_i/m_e (for O^+ ions), typical computations, covering 20,000 time steps, require about a factor of 10 longer time than corresponding cases with no flow and B=0, where $m_i=m_e$ was used. In addition, the electron gyro motion now needs to be resolved, although, since the gyro time is longer than the plasma time, this does not further limit the choice of time step. Figure 10 shows the computed distributions of electron and ion densities, net charge density and potential, for a case with cross-flow, but no B field. Several new features are prominent:

(a) A nearly void wake, created by the repulsion of ions by the positive tether, and the exclusion of electrons due to the wake's negative potential.

(b) What appears to be a "bow shock", but is really a "caustic surface" tangent to the deflected ions' trajectories, so that the ion (and also electron) density is enhanced in it by factors up to 2-4.

15

(c) The location of the sheath edge (frontal part) at a potential of about 5 eV, corresponding to the energy of the incoming directed ion beam. This is much higher than the plasma thermal energy (0.1eV), and implies the existence of an extended quasi-neutral region where electrons are accelerated to supra- thermal velocity through a background of slowed-down ions. This should lead to a strong two-stream instability, the consequences of which we are now exploring (see below).

Figure 11 displays a similar case, but with a transverse B=0.3 Gauss field added. The wake is now narrower, and there is a wing-like extension of the quasi-neutral presheath, extending along the magnetic lines. The strong caustic density ridge persists, and the sheath's edge is still at 5 eV.

The top two panels in Figure 12 show time records of electron collection by the tethers of Figures 10 and 11. The most striking result is that both cases collect current well in excess of the Orbital Motion Limit, more so in the magnetized case of Figure 11. As explained in Sec. 3.2, this should not occur, on general grounds, and one of the goals of the proposed research is to understand clearly the physics behind this result (as well as to verify beyond doubts its accuracy.

One intriguing possibility is illustrated in the two lower panels of Figure 12, which show the results of a numerical experiment where the plasma oscillations which are always present in the computation are frozen for periods of 100 time steps (10-20 plasma periods) at a time, while particles continue to be pushed. Of course, this has no real physical meaning, and was done only to verify that particles conserve energy when the fields are steady (they do). But what was found in addition is that, with the oscillations absent, the current collection drops (on average) to the OML limit or below. This is strongly reminiscent of the arguments of Cooke and Katz[21], and is consistent with our observation about the two-stream unstable region in the presheath. More detailed work is clearly needed here.
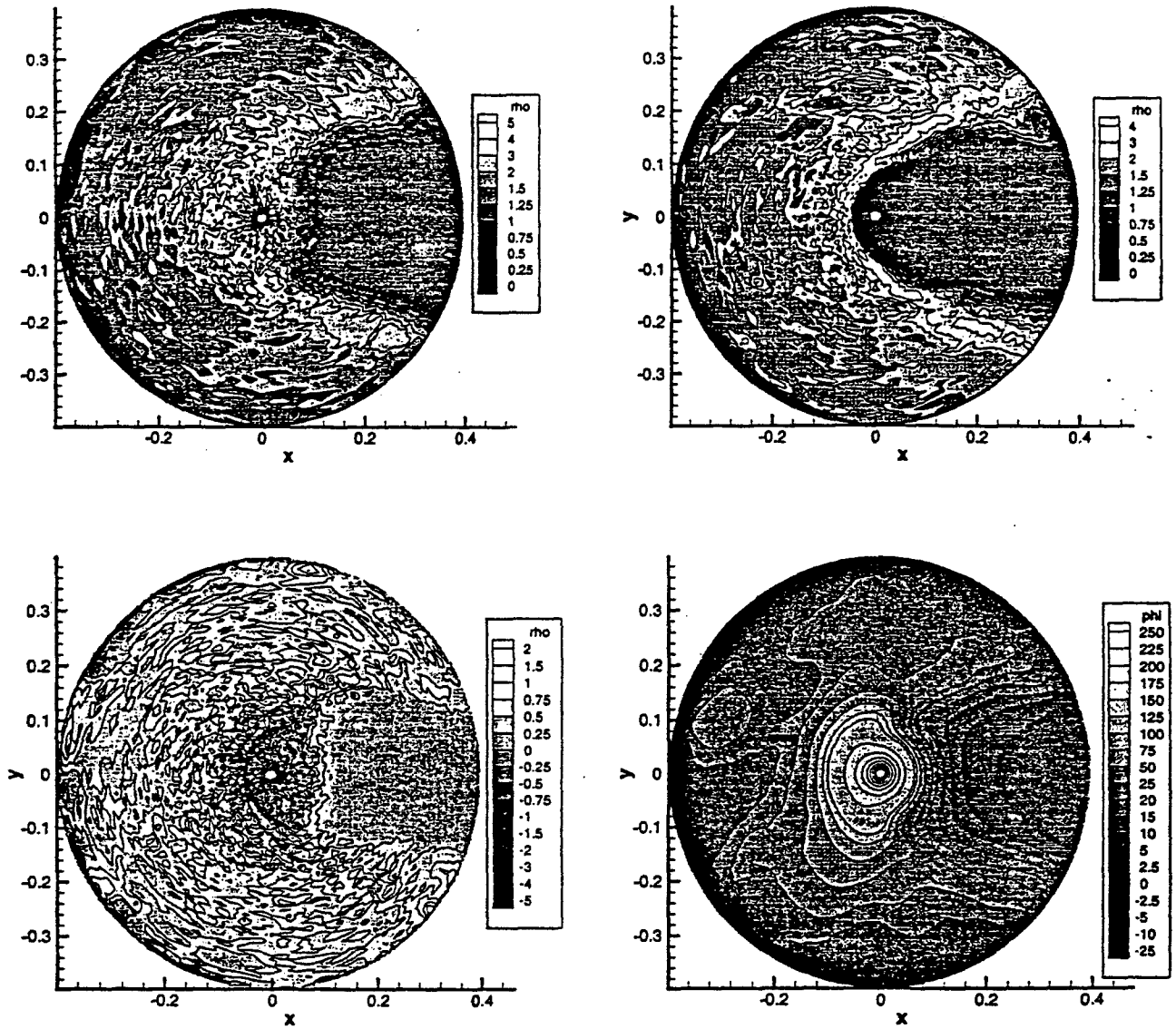
Figure 10: Computed distributions for a case with cross-flow (8000 m/s.) but no magnetic field. Top left: n_e/n_∞. Top right: n_i/n_∞. Bottom left: $(n_i - n_e)/n_\infty$. Bottom right: $\phi/(0.1eV)$. The tether potential is 25V, the ion and electron temperatures are 0.1eV, $n_\infty = 10^{11} m^{-3}$, and R/d$_{Debye}$=1. Distances are shown in m.
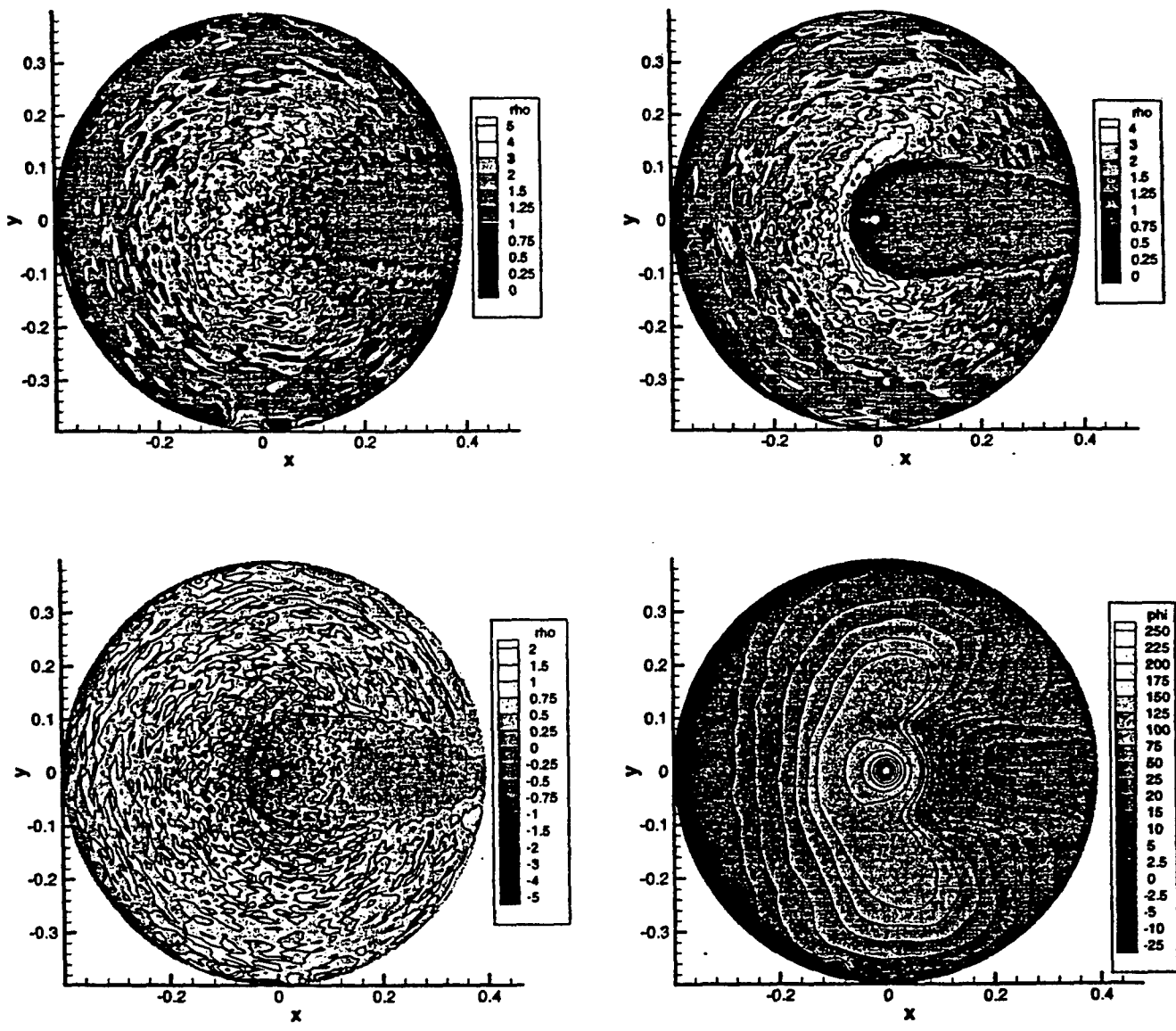
Fig 11: Computed distributions for a case with both, cross-flow, and a magnetic field perpendicular to both, the tether and the flow. Conditions as in Fig. 5, plus B=0.3 Gauss.
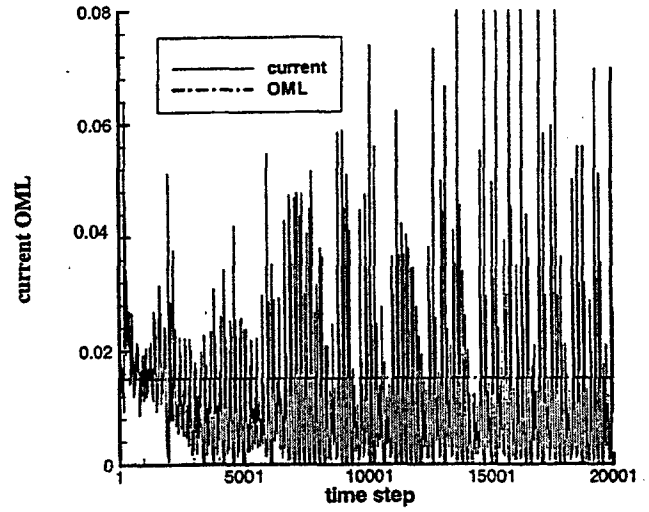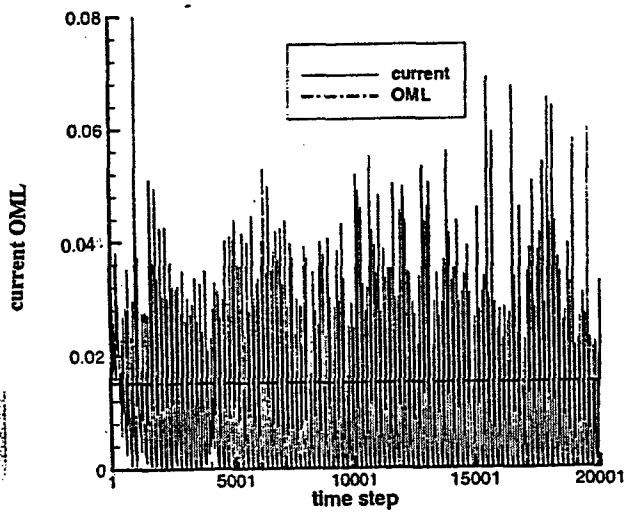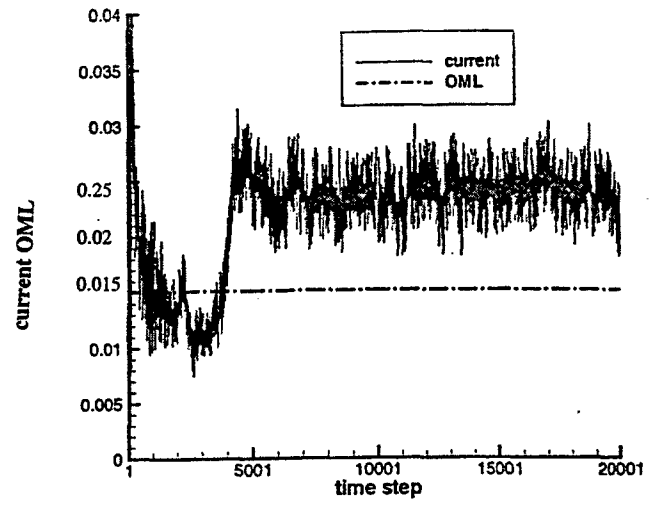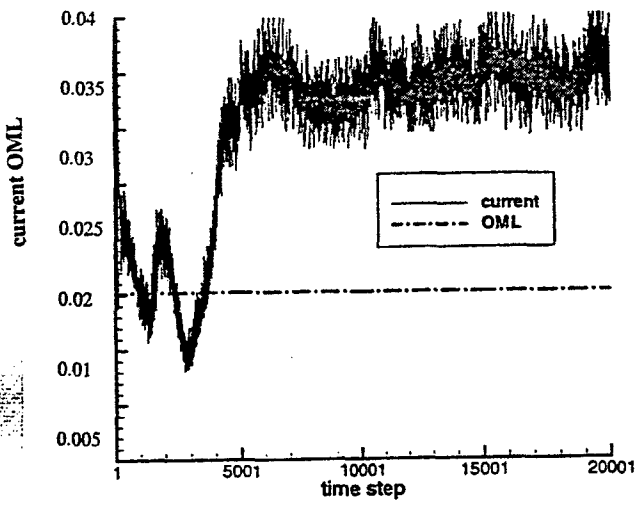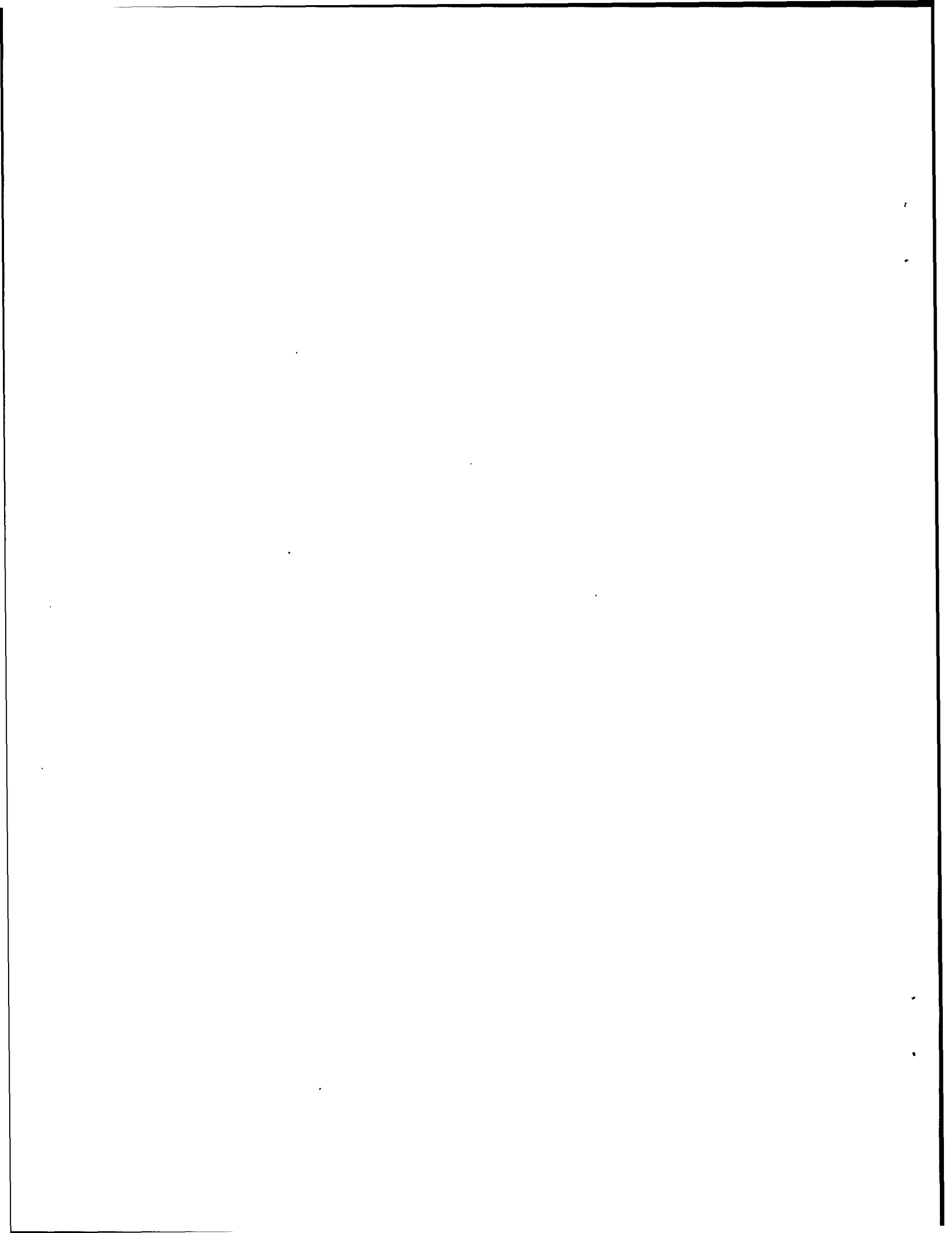
Fig. 12: Time evolution of collected current for the cases of Figs. 5 and 6. Top left: magnetized; top right: unmagnetized. Bottom left and right are as the top row, but the potential was artificially frozen during periods of100 time steps at a time. The horizontal dot-dash lines show the OML current for these cases.

19

References

1. Shaw, G.G., <u>Analysis of the Ion Current Collection in the Plasma Wake during the CHAWS-I Experiment</u>, M.S. Thesis, MIT, (Aero/Astro), 1995.

2. Giffin, G.B., <u>Analysis of the Ion Current Collection in the plasma Wake during the CHAWS Experiments</u>, M.S. Thesis, MIT (Aero/Astro), June 1997.

3. Giffin, G.G., Hastings, D.E., Font, G.I. and Shaw, G.B., "Particle-in-Cell Analysis of Charging Hazards and Wake Studies Experiment." J. of Spacecraft and Rockets, Vol. 35, no. 3, May-June 1998, pp. 395-402.

4. Cooke, D.L., Enloe, C.L., Pakula, W.A., Violet, M.D., Tate, M.F., Roth, C., Bonito,I.N., Giffin, G.B. and Shaw, G.B., "Current-Voltage Data for the CHAWS Space Flight Experiment". U.S. AF Phillips Lab, PL-TR-97-2066 Hanscom AFB, MA. Feb. 1997.

5. Enloe, C.L., Cooke, D.D., Pakula, W.A., Violet, M.D., Hardy, D., Chaplin, C.B., Kirkwood, R., Tautz, M.F., Bonito, N., Roth, C., Courtney, G., Davis, V.A., Mandell, M.J., Hastings, D.E., Shaw, G.B., Giffin, G.B. and Sega, R.M., "High Voltage Interactions in Plasma Wakes: Results from the CHAWS Flight Experiments". J. of Geophysical Research, Vol. 102, No. A1, 1997, pp. 425-433.

6. Chan, Chung, "Experimental Results on Ion-Induced Secondary Emission on the CHAWS Probe Cover." Northeastern Univ., Quarterly Report to Phillips Lab, 1995.

7. Grossi, M.D. Tether History and Historiography. Italian Physics Society Conference Proceedings, Vol. 14, 3-8, 1987.

8. Clarke, A.C. The Space Elevator – Thought Experiment or Key to the Universe, Reissue of a 1963 paper in Advances in Earth Oriented Applications of Space Technology, Vol. I, 39-48, 1981.

9. Artsutanov, Yu., Space Electrodynamics, Translated from Komsomolskaya Pravda, 1960.

10. Martinez-Sanchez, M. and Hastings, D.E., A Systems Study of a 100 kW Electrodynamic Tether, The Journal of Astronautical Sciences, Vol. 35, 75-96, 1987.

11. L. Johnson and M. Herrmann, <u>International Space Station, Electrodynamic Tether Reboost Study</u>, NASA/TM-1998-208538, July 1998.

12. Estes, R.D., Lorenzini, E.C., Sanmartin, J., Pelaez, J., Martinez-Sanchez, M. Johnson, L. and Vas, I., "Bare Tethers for Electrodynamic Space Station Propulsion". Submitted to the AIAA J. of Propulsion and Power, Sep. 1998.

13. Gilchrist, B.E., Johnson, L. and Bilen, S.G., "Space Electrodynamic Tether Propulsion Technology: System Considerations and Future Plans", paper AIAA 99-2841, 35th Joint Propulsion Conf., Los Angeles, CA, June 1999.

14. Laframboise, J.G., "Theory of Spherical and Cylindrical Langmuir Probes in Collisionless Maxwellian Plasma at Rest". University of Toronto, Institute of Aerospace Studies, Report no. 100, 1966.

15. Johnson, L., Gilchrist, B., Estes, R., Lorenzini, E. and Balance, J., "Propulsive Small Expendable Deployer System (ProSeds) Space Experiment", paper 98-4035, 34th Joint Propulsion Conf., Cleveland, OH, 1998. (See also paper of some title in the Proc. of the Tether Technology Interchange Meeting, NASA CP-1998-206900, pp. 103-108, 1998.

16. Sanmartin, J.R., Martinez-Sanchez, M. and Ahedo, E., "Bare Wire Anodes for Electrodynamic Tethers". Journal of Propulsion and Power, Vol. 9, No. 3, pp. 353-360, 1993.
17. Sanmartin , J.R. Sanmartin and Estes, R.D., "The Orbital Motion Limited Regime for Cylindrical Langmuir Probes", Physics of Plasmas, Vol. 6, no. 1, pp. 395-405, Jan. 1999.
18. J.R. Sanmartin and R.D. Estes, "Collection Effects in Close Parallel Bare Tethers", paper AIAA 2000-1073, 38th Aerospace Sc. Meeting, Reno, NV, Jan 00.
19. J.G. Laframboise and L.W. Parker, "Probe Design for Orbit-Limited Current Collection". Phys. Fluids, Vol. 16, 629 (1973).
20. J.G. Laframboise, "Current Collection by a Positively Charged Spacecraft: Effects of its Magnetic Presheath". J. Geophysical Res., Vol. 102, 2417 (1997).
21. D.L. Cooke and I. Katz, "TSS-1R Electron Currents: Magnetic –Limited Collection from a Heated Pre-Sheath". Geophysical Research Letters, Vol. 25, No. 5, pp. 753-756, March 1998.
22. L.W. Parker and B.L. Murphy, "Potential Buildup on an Electron-Emitting Ionospheric Satellite". J. Geophysical Res., Vol. 72, 1631 (1967).
23. T. Tajima, Computational Plasma Physics, with Applications to Fusion and Astrophysics. Addison Wesley, Frontiers in Physics series (1989).
24. C.K. Birdsall and A.B. Langdon, Plasma Physics via Computer Simulation. Institute of Physics Publishing, Bristol and Philadelphia (1991).
25. T. Onishi and M. Martinez-Sanchez, "Bare Wire Current Collection Using a Particle-in-Cell (PIC) Method". Post-deadline poster paper at the Tether Technology Interchange meeting (NASA, Marshall SFC, September 9-10, 1997).
26. T. Onishi, Electron Current Collection by a Positively Charged Tether, Using a Particle-in-Cell Method. Master's Thesis, MIT (Aeronautics/Astronautics) May 1998.
27. J.W. Schummer and J.P. Holloway, "Vlasov Simulations Using Velocity-Scaled Hermite Representations". J. of Computational Physics, 144, 626-661 (1998).
28. T. Onishi, M. Martinez-Sanchez and D.L. Cooke, "Computation of Current to a Moving Bare Tether". Paper IEPC 99-217, 26th IEPC Conference, Kitakyushu, Japan, Oct. 1999.